

Quantum Monte Carlo simulations of the attractive SU(3) Hubbard model on a honeycomb lattice

Han Xu,^{1,2} Zhichao Zhou,¹ Xin Wang,² Lei Wang,³ and Yu Wang^{1,*}

¹*School of Physics and Technology, Wuhan University, Wuhan 430072, China*

²*Department of Physics, City University of Hong Kong,
Tat Chee Avenue, Kowloon, Hong Kong SAR, China,*

and City University of Hong Kong Shenzhen Research Institute, Shenzhen, Guangdong 518057, China

³*Institute of Physics, Chinese Academy of Sciences, Beijing 100190, China*

We perform the projector quantum Monte Carlo simulation of the half-filled attractive SU(3) Hubbard model on a honeycomb lattice, exploring the effects of SU(3) symmetry on the correlated attractive Dirac fermions. Our simulation indicates the absence of pairing order in the system and shows a quantum phase transition from the semimetal to charge density wave (CDW) at the critical point $U_c = -1.52(2)$. We demonstrate that this quantum phase transition belongs to the chiral Ising universality class according to the numerically determined critical exponents $\nu = 0.82(3)$ and $\eta = 0.58(4)$. With the increase of coupling strength, the trion formation is investigated, and the change in probability of the on-site trion occupancy infers the coexistence of on-site trionic and off-site trionic CDW states at half-filling.

I. INTRODUCTION

With the high development of the experiment, optical lattices loaded with ultracold atoms has become an excellent lab for studying strong correlation physics. Unlike those in solids, physical parameters in an optical lattice system, e.g. lattice structure and on-site interaction, are highly controllable and continuously adjustable, which opens an avenue for simulating various Hamiltonians with ultracold atoms. Interestingly, ultracold alkali and alkaline-earth fermions carry large hyperfine spins, which provides an opportunity to study SU(N) ($N > 3$) symmetries that are typical in the high energy context but rare in solids. In condensed matter physics, the previous study of lattice fermion or spin models with SU(N)[1–3] or Sp(N)[4, 5] symmetry, was essentially a theoretical effort to handle strong correlations by employing a systematic $1/N$ expansion. In recent decade, fermionic models with SU(N) symmetry have been of great interest to both experimentalists [6–13] and theorist [14–17] in the context of ultracold atoms.

When the number of flavor components N increases, the quantum fluctuations are enhanced, and consequently the physics can be dramatically different between SU(N) models and their SU(2) counterparts. In the SU(N) models, there may exist exotic states of matter which are not stable or accessible in SU(2) systems like solids. The SU(3) models, the minimal model with SU(N) symmetry, should reveal the smallest difference between SU(N) system and its SU(2) counterpart. In experiment, the SU(3) symmetry can be realized by loading ^6Li atoms into the optical trap [18–21]. It is proposed that in the attractive SU(3) Hubbard model away from half filling, a color superfluid (CSF) state exists in the weak coupling regime [15, 22], and a trion state is formed

in the strong coupling regime [22, 23]. This interaction-induced phase transition between the color superfluid state and the trion state has been extensively studied at the mean-field level [22–24]. Interestingly the phase transition in the SU(3) attractive Hubbard model mimics the transition between quark superfluid and baryonic phase in quantum chromodynamics [22, 23, 25–27]. Numerical simulations by using dynamical mean-field theory have shown a phase transition from a color superfluid state to a charge density wave (CDW) state in the dimension of $d = \infty$ at half filling [28, 29]. Exact diagonalization study of a small-sized chain at quarter filling demonstrates the local trion formation and the crossover from the suppressed pairing order into the trionic regime [30].

The projector quantum Monte Carlo (PQMC) method is a nonperturbative technique which is basically unbiased and asymptotically correct. The PQMC simulations of the SU(2) attractive Hubbard model are sign-problem-free, regardless of the degree of filling [31, 32]. However, due to notorious sign problem a PQMC study of the attractive SU(3) Hubbard model has long been absent in literature. Until recently advances in the PQMC algorithm eliminated the sign problem in the attractive SU(3) Hubbard model at half filling [33–35]. In this paper, we shall implement this algorithm to perform the PQMC simulation of the half-filled attractive SU(3) Hubbard model on a honeycomb lattice, exploring the effects of SU(3) symmetry on the correlated attractive Dirac fermions.

The rest of this paper is organized as follows. In Sec. II, the model Hamiltonian and the scheme of PQMC simulations are introduced. In Sec. III, the ordering associated with the ground state is investigated, and then the quantum phase transition between semi-metal and CDW is studied. The trion formation is also discussed. The conclusions are drawn in Sec. IV.

* yu.wang@whu.edu.cn

II. MODEL AND METHOD

The half-filled SU(3) Hubbard model is defined by the lattice Hamiltonian:

$$H = -t \sum_{\langle ij \rangle, \alpha} (c_{i\alpha}^\dagger c_{j\alpha} + \text{h.c.}) + \sum_{i, \alpha < \beta} U (n_{i\alpha} - \frac{1}{2})(n_{i\beta} - \frac{1}{2}), \quad (1)$$

where t is the hopping amplitude; $\langle i, j \rangle$ denotes a pair of nearest-neighbor sites on a square lattice; α and β are the flavor indices running from 1 to 3; $n_{i\alpha} = c_{i\alpha}^\dagger c_{i\alpha}$ is the particle number operator for color α on site i ; $U < 0$ describes the attractive on-site interaction. The chemical potential equals zero at half filling due to the particle-hole symmetry of the above Hamiltonian.

In the strong coupling limit ($t/|U| \ll 1$), the CDW long-range order dominates [22, 23] and the BEC in the CDW regime is not stable in the SU(3) system [30]. N fermions form a local bound color singlet in one sublattice and leave the other sublattice empty, which breaks the lattice symmetry as shown in Fig. 1(a). The energy of the system is increased by $-\frac{(N-1)U}{2}$ when an extra particle (hole) is added to the system. However, due to the Pauli exclusion principle, the extra particle (hole) can hop on a triangular lattice via second-order superexchange process as shown in Fig. 1(a), which expands the excitation energy level into an energy band and then decreases the energy gap to $\Delta_E \approx -\frac{(N-1)U}{2} - W$, where $W \approx -\frac{6t^2}{(N-1)U}$, inverse proportional to the number of flavor components $N-1$ (see Appendix C). We then obtain the critical value U_c at which the energy gap Δ_E vanishes,

$$U_c \approx -\frac{2\sqrt{3}t}{N-1}, \quad (2)$$

We shall see that the factor of $N-1$ also appears in the single-particle spectrum and the CDW gap function based on the static mean-field theory [36].

In the mean-field approximation, the particle number on each site is $\langle c_{i\alpha}^\dagger c_{i\alpha} \rangle = \varepsilon^i \Delta$ where Δ is the CDW order parameter, ε^i takes the value of $+1$ in one sublattice and -1 in the other to characterize the density imbalance with respect to the two sublattices. The mean-field CDW order parameter can be rewritten as an average over lattice sites,

$$\Delta = \frac{1}{2L^2N} \sum_{i, \alpha} \varepsilon^i \langle c_{i\alpha}^\dagger c_{i\alpha} \rangle. \quad (3)$$

After decoupling the on-site interaction by an on-site external field $\varepsilon^i \Delta$ and applying the Fourier transformation to Eq. (1), the mean-field Hamiltonian in the momentum space becomes $H_{\text{MF}} = \sum_{k, \alpha} \hat{\psi}_{k, \alpha}^\dagger \hat{h}_k \hat{\psi}_{k, \alpha}$ where,

$$\hat{h}_k = \begin{bmatrix} (N-1)U\Delta & \epsilon_k^\dagger \\ \epsilon_k & (1-N)U\Delta \end{bmatrix}. \quad (4)$$

Here, $\epsilon_k = -t \sum_{e_j} e^{-ik \cdot e_j}$, e_j sums over three vectors $e_1 = (0, 1)$, $e_2 = (-\frac{\sqrt{3}}{2}, -\frac{1}{2})$, $e_3 = (\frac{\sqrt{3}}{2}, -\frac{1}{2})$ and the distance between nearest-neighboring sites is taken as the unit of length. At half filling, the value of Δ satisfies the following equation,

$$\Delta = \frac{1}{2L^2N} \sum_{k, \alpha} \left(1 - \frac{\epsilon_k^2}{|\lambda_k|^2 - (N-1)U\Delta|\lambda_k|} \right), \quad (5)$$

where $\lambda_k = \pm \sqrt{(N-1)^2 U^2 \Delta^2 + \epsilon_k^2}$ are the eigenvalues of \hat{h}_k . As we can see, a finite value of Δ opens the energy gap $-2(N-1)U\Delta$ in the single-particle spectrum, so Eq. (3) is often called *the gap function*.

The value of Δ can be solved by the root-finding method [37, 38] and the results are shown in Fig. 1. The critical value for SU(3) case is $U_c^{\text{MF}} \approx -1.11t$, similar to the prediction of Eq. (2). Notice that the change in fermion components only affects the right-hand side of Eq. (5). More precisely, it changes the energy scale of U by a factor of $N-1$ [36]. One can test this statement through the critical value for the SU(2) case, $U_{c,2}^{\text{MF}} = 2U_c^{\text{MF}} \approx -2.23t$, which is consistent with the result in [39].

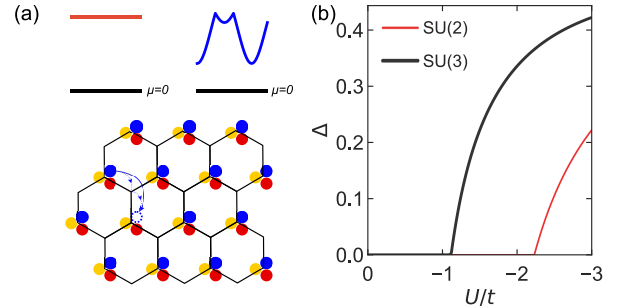


FIG. 1. (a) On the background of the half-filled trionic CDW state, the energy dispersion relation to add one particle at the limit (upper left) $t/U = 0$, (upper right) $t/U \ll 1$, and (lower) the sketch of a hole hopping and the spatial arrangement of trions. (b) The CDW order parameter Δ as a function of the attractive interaction U for the SU(2) and SU(3) model at half filling. (c) Attractive SU(2) and (d) attractive SU(3) Hubbard model on two sites where the particles can hop with amplitude t . The on-site interaction brings down the energy by $(N-1)|U|$ for particles on the same site.

PQMC in the determinant formalism [40–42] is used and the half-filled attractive SU(3) Hubbard model is sign-problem-free with the auxiliary field [33–35] adopted in this work. The details on designing the auxiliary field are discussed in Appendix A. We choose the lattice size $L = 3n$ ($n = 1, 2, \dots$) that contains the Dirac points in its reciprocal lattice and impose the periodic boundary condition along the x and y directions to preserve the translational symmetry. The trial wave function is chosen as the ground state of the noninteracting part with the anti-periodic boundary condition to break the degeneracy at the Dirac points. The projection time $\beta = \frac{8}{3}L$ and

Suzuki-Trotter discretization $\Delta\tau \leq 0.1$ in the projection time are sufficient to give accurate ground-state properties of the system. When calculating unequal-time correlations, $\beta = \frac{10}{3}L$ is adopted. Physical observables are measured around $\frac{\beta}{2}$. The auxiliary-field QMC method for the SU(2) Hubbard model has the computational complexity $\frac{\beta}{\Delta\tau} (2L^2)^3$ while our method decouples the Hubbard interaction into the on-site flavor-filp forms, which increases the computational complexity to $\frac{\beta}{\Delta\tau} (6L^2)^3$. The computational complexity of our method is further explained in Appendix A. The maximum lattice size we simulated is $L = 12$. We take the hopping amplitude $t = 1$ throughout our following discussions.

III. RESULTS

A. Absence of the pairing order

For the intermediate values of U , the fermion composite from strong coupling breaks up to a Cooper pair and an unpaired free fermion, which breaks the SU(3) symmetry of the trionic state to SU(2) symmetry, and induces the color superfluid state [22]. DMFT methods have been extensively applied to the phase transition, domain formation and stability of the CSF phase [28, 29, 36]. In order to study the superfluid (SF) order, we first calculate the uniform pairing structure factor at Γ point,

$$S_{\text{pair}}(L) = \frac{1}{2L^2} \sum_{i,j} P(i,j), \quad (6)$$

where $2L^2$ is the number of lattice sites and $P(i,j)$ is the two-point equal-time pair-pair correlation function, $P(i,j) = \sum_{\alpha < \beta} \langle c_{i\alpha}^\dagger c_{i\beta}^\dagger c_{j\beta} c_{j\alpha} + c_{i\beta} c_{i\alpha} c_{j\alpha}^\dagger c_{j\beta}^\dagger \rangle$ [32]. Extrapolating the structure factor to thermodynamic limit, the long-range SF order parameter is obtained: $P_s = \lim_{L \rightarrow \infty} \sqrt{\frac{1}{2L^2} S_{\text{pair}}(L)}$. We note that at the non-interacting limit ($U = 0$) the structure factor equals to 3.

As shown in Fig. 2(b), the numerical results at $U = -0.05$, near the non-interacting limit, show good agreement with the analytic value of the structure factor. Tuning on the attractive on-site interaction, the SF order parameter on the finite-size lattice has maximum at the intermediate $|U| \approx 2$. However, the simple extrapolation of the pairing order parameter $P_s(L)$ shows no sign of SF ordering, which is presented in Fig. 2(a). This is quite different from the SU(2) case: for the half-filled SU(2) attractive Hubbard model, the attractive interaction induces the quantum phase transition from semi-metal to the ordered phase where the s-wave pairing phase and CDW phase are degenerate due to the hidden pseudo-spin symmetry [32]. Away from half filling, the pairing order dominates and only short-range CDW correlation occurs [31] where the BCS-BEC crossover phenomenon appears [32, 43].

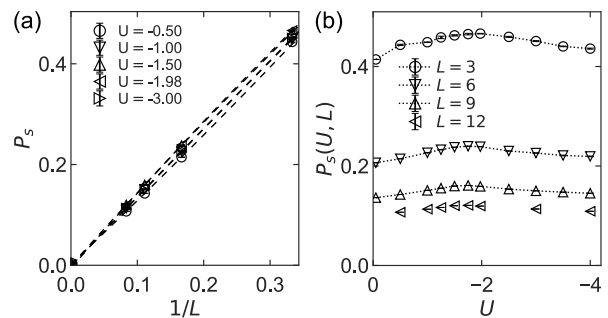


FIG. 2. The SF order in the attractive SU(3) Hubbard model. (a) Extrapolation of the SF order to thermodynamic limit for different U . Error bars are smaller than symbols. Dashed lines are the least-square fits with the quadratic polynomials in $\frac{1}{L}$. (b) Evolution of the SF order as a function of U for finite lattice sizes $L = 3, 6, 9$ and 12 . Dotted lines are guides to eyes.

B. Formation of the CDW order

At strong coupling, analytic results and exact numerical evidences prove a stable CDW phase [23, 28, 30, 36] where three fermions tend to form a trion which is a spinless fermion of binding energy $3|U|$. The model's low-energy physics can be seen as an effective spinless fermion model with nearest-neighbor hopping and nearest-neighbor repulsive interaction,

$$H_{\text{eff}} = -\tilde{t} \sum_{\langle ij \rangle} (c_i^\dagger c_j + h.c.) + \tilde{V} \sum_{\langle ij \rangle} n_i n_j \quad (7)$$

where $\tilde{t} \sim \frac{t^3}{U^2}$ and $\tilde{V} \sim -\frac{t^2}{U}$ [28, 30]. The cube of t in the effective hopping amplitude \tilde{t} comes from that moving a trion requires three fermion hopping processes [30]. The effective hopping amplitude vanishes in $d = \infty$ dimension and trion becomes immobile [22, 23, 28]. On a honeycomb lattice that has finite lattice dimension, trion becomes mobile. The system undergoes the competition between the trionic Fermi liquid and CDW phase where the energetically favorable configuration is one trion for each unit cell due to repulsive interaction \tilde{V} [22, 23, 28]. The stabilization of Fermi liquid against the CDW ordering at half filling is illustrated by the half-filled spinless fermion model Eq. (7), and the QMC simulations have been applied to study the quantum phase transition between semi-metal and CDW phase in [44, 45]. We note that if we tune $\tilde{t} \rightarrow t$, the effective repulsive term changes like $\tilde{V} \rightarrow |U|$.

We first need to calculate the staggered charge structure factor defined at Γ point,

$$S_{\text{CDW}}(L, \Gamma) = \frac{1}{2L^2} \sum_{i,j} \varepsilon^i \varepsilon^j C(i,j), \quad (8)$$

where $C(i,j) = \sum_{\alpha, \beta} \langle n_{i\alpha} n_{j\beta} \rangle$ is the density-density correlation function. Then, the order parameter of CDW

phase is given by $D = \lim_{L \rightarrow \infty} \sqrt{\frac{1}{2L^2} S_{\text{CDW}}(L, \Gamma)}$. At the non-interacting limit, the structure factor has an analytic value $\frac{3}{2}$. Near the critical point, considering only to the first-order approximation, the scaling functions on which the order parameters on finite-size lattices collapse below and above the critical point are [44–47],

$$S_{\text{CDW}}(\delta u; L) = L^{1-\eta} \tilde{S}_{\text{CDW}}(\delta u L^{1/\nu}) \quad (9)$$

$$D(\delta u; L) = L^{\frac{\zeta}{\nu}} \tilde{D}(\delta u L^{\frac{1}{\nu}}), \quad (10)$$

where $\delta u = U - U_c$ is the deviation from the critical value. Substituting the scaling functions Eq. (9) and Eq. (10) to the definitions of the structure factor and the order parameter, we obtain the relation $\eta = -2\frac{\zeta}{\nu} - 1$.

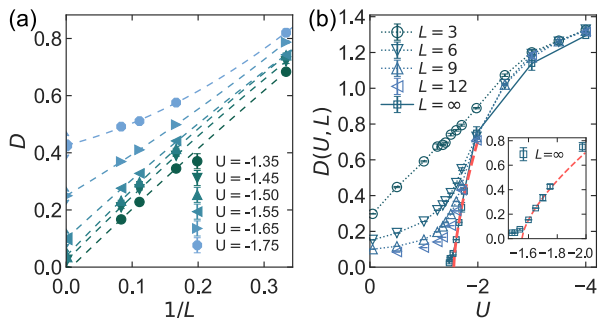


FIG. 3. The CDW order in the attractive SU(3) Hubbard model. (a) Extrapolation of the SF order to thermodynamic limit for different U . Dashed lines are the least-square fits with the quadratic polynomials in $\frac{1}{L}$. (b) Evolution of the CDW order as a function of U for finite lattice sizes: $L = 3, 6, 9$ and 12 . Dotted lines are guides to eyes. The $L = \infty$ curve represents the extrapolated data and the red color dashed curve is the fit to $D \sim |U - U_c|^{-\zeta}$. The inset shows enlarged plots near the critical point.

In Fig. 3(a), the extrapolation of CDW order parameter is performed under various U , where a finite value appears around the critical value $U_c \approx -1.5$ indicating the CDW phase transition. Fig. 3(b) shows the CDW order parameter, $D(L)$, increases monotonically when increasing the attractive on-site interaction. Numerical results at $U = -0.05$ show good consistency with the analytic value at the non-interacting limit. For the attractive interaction $|U| \geq 3$, the value of $D(L)$ is approximately size-independent, which indicates the CDW correlation length is larger than the lattice size used in our simulation. This is a strong evidence of the existence of CDW order at strong coupling and the formation of CDW order rules out the existence of the trionic Fermi liquid. We note that the critical point is $U_c^{\text{MF}} \approx -1.11$ at mean-field level when quantum fluctuations are neglected. On the other hand, it requires stronger coupling to form an ordered state with the presence of quantum fluctuations; thus $|U_c^{\text{MF}}| < |U_c|$. The increase in the critical interaction strength also appears in the SU(2) case: $|U_{c,2}^{\text{MF}}| < |U_{c,2}|$ where $|U_{c,2}| \approx 3.85$ [48].

Suppose the extrapolated CDW order parameter near the critical point follows the standard power-law behavior

$D \sim |U - U_c|^{-\zeta}$ [45, 47]. We obtain the critical exponent $\zeta = -0.67(3)$ and the critical point $U_c = -1.55(1)$, as shown in the inset of Fig. 3(b). We notice that the CDW order parameter have a tail of data with small non-zero values, for example the first three data points in the inset. The non-vanishing extrapolated values presumably come from the simple $1/L$ extrapolation [46, 47] and should be excluded from our curve-fitting.

C. Nature of the CDW phase transition

The phase transition of interacting gapless Dirac fermions are described by the Gross-Neveu model [49, 50]. Large-scale PQMC simulations have been widely employed to the critical phenomena of Dirac fermions on a lattice model, featuring the quantum phase transition from semi-metal phase to CDW phase. For example, for SU(2) attractive Hubbard on a honeycomb lattice with increasing U , the relevant quantum phase transition belongs to the $N_s = 8$ chiral Heisenberg universality class [48, 51]. Here N_s denotes the spinor components [50]. For SU(3) case, the effective model in the strong coupling regime is a spinless one (trion) described by Eq. (7). The spinless Dirac fermions on a honeycomb and a π -flux square lattices possess such kind of quantum phase transition from semi-metal to CDW by increasing the nearest-neighboring repulsion \tilde{V} . The relevant quantum phase transition belongs to the $N_s = 4$ chiral Ising universality class [44, 45, 52]. Furthermore in our problem, both the semi-metal phase and the CDW phase preserve the SU(3) symmetry, and the absence of pairing order keeps the SU(3) symmetry invariance. So we expect that the quantum phase transition between semi-metal and CDW phase discussed above belongs to the chiral Ising universality class.

We first use the dimensionless correlation ratio to locate the critical point [53, 54],

$$R_{\text{CDW}} = 1 - \frac{S_{\text{CDW}}(L, \Gamma + \delta \mathbf{k})}{S_{\text{CDW}}(L, \Gamma)}, \quad (11)$$

where $\delta \mathbf{k}$ represents the shift in the reciprocal lattice. At strong coupling when forming the CDW order, $S_{\text{CDW}}(L, \Gamma)$ is much larger than $S_{\text{CDW}}(L, \Gamma + \delta \mathbf{k})$ so R_{CDW} approaches unity. At weak coupling, R_{CDW} approaches zero due to the absence of CDW order. The dimensionless ratio satisfies the scaling function,

$$R_{\text{CDW}}(\delta u; L) = \tilde{R}_{\text{CDW}}(\delta u L^{\frac{1}{\nu}}). \quad (12)$$

Thus, at the critical point, R_{CDW} is a size-independent variable for sufficiently large L . In Fig. 4, the $R_{\text{CDW}}-U$ curves of different lattice sizes cross in the region $-2.0 < U < -1.5$ where the crossings slightly drift when changing L . We use the resampling method to locate the intersection points $U_c(L)$ with respect to the $L, L+2$ curves, and we use the least-square fit to the coupling strength with the function, $U_c(L) = U_c + aL^{-b}$ [51]. The

extrapolation gives the critical value $U_c = -1.52(2)$ and the fitting parameter $b = 2.2(3)$.

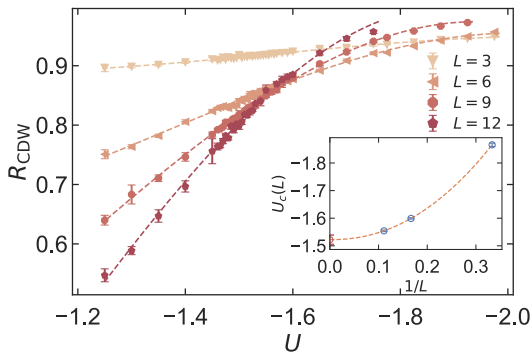


FIG. 4. Correlation ratio R_{CDW} for finite lattice sizes $L = 3, 6, 9$ and 12 close to the phase transition point. The intersection points are calculated using the cubic polynomials from many times of resampling of the data accordingly. Dashed lines are one example of the cubic polynomial fits. The inset shows the extrapolation of the intersection points from least-square fit with $U_c(L) = U_c + aL^{-b}$ using absolute errors estimated with the resampling method.

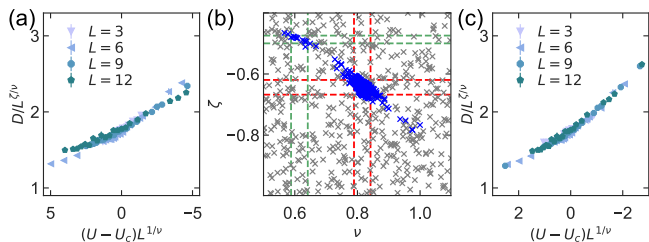


FIG. 5. Scaling collapse of the CDW order parameter $D(L, U)$. The exponents are (a) $\nu = 0.61(3)$, $\zeta = -0.49(2)$ and (c) $\nu = 0.82(3)$, $\zeta = -0.64(3)$. We set the critical value $U_c = -1.52$. (b) Best-fitting analysis of the critical exponents. Gray points are the initial guesses and the blue points are the best-fitting outputs. The green lines and the red lines denote the standard error of the outputs around $\nu = 0.6$ and $\nu = 0.8$, respectively.

We next calculate the critical exponents from the best-fitting procedure adapted in [55, 56] from the CDW order parameter. Based on the scaling function Eq. (10), we randomly sample the critical value in the parameter region around $U = -1.52$, randomly choose the initial guesses of the exponents, ν_0, ζ_0 , inside a small range [47, 48]. As shown in Fig. 5(b), we note that there seems to have two possible solutions: the critical exponents denoted by pairs of green lines are estimated as $\nu = 0.61(3)$, $\zeta = -0.49(2)$ and the one denoted by pairs of red lines are estimated as $\nu = 0.82(3)$, $\zeta = -0.64(3)$. We show the scaled CDW order parameter with the two pair of exponents in Fig. 5(a) and Fig. 5(c). Their reduced χ^2 evaluations are 10.71 and 4.037 where χ would have the value close to one if the data really collapses to a scaling function [57]. Apparently, the second pair of exponents is a more reliable result. For comparison, the standard

power-law assumption in Sect. III B induces somewhat bigger values of U_c and $-\zeta$ because of the extrapolation method and finite lattice sizes. Nevertheless, from the best-fitting analysis on the CDW order parameter, the critical exponents are $\nu = 0.82(3)$, $\zeta = -0.64(2)$ and $\eta = 0.58(4)$. Our results are consistent with the QMC results on the $N_s = 4$ chiral Ising model [44, 45, 58]. Our results are also in agreement with the RG calculations: $\nu = 0.74 \sim 0.93$ and $\eta = 0.50 \sim 0.64$ [59–62] but is slightly different from the perturbative calculations: $\nu = 0.87 \sim 1.04$ and $\eta = 0.4 \sim 0.5$ [50] just like other QMC simulations [45, 58].

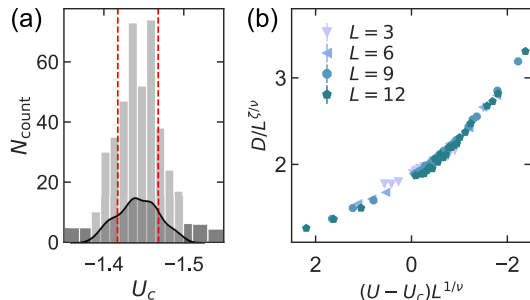


FIG. 6. (a) Best-fitting analysis of the critical value U_c with the exponents fixed: $\nu = 1.02(3)$ and $\zeta = -0.90(5)$. The red lines show the standard error of the critical value. Initial guesses of U_c are shown by the gray color normalized histogram. The fitting outputs are shown by the silver color histogram and the black color curve as the kernel density estimate. (b) Scaling collapse of the CDW order parameter $D(L, U)$ using exponents $\nu = 1.02$, $\zeta = -0.9$ and $U_c = -1.44$.

We finally test the critical exponents $\nu = 1.02(3)$ and $\zeta = -0.90(5)$ of the $N_s = 12$ chiral Ising universality class [50]. Following the same procedure above, we obtain the critical value $U_c = -1.44(3)$ which is incompatible with the previous results, and the scaling collapse is shown in Fig. 6(b) where the reduced χ^2 evaluations is 5.075. Additionally, for the scaling collapse of the dimensionless ratio, we should multiply the first-order correction, $1 + cL^{-\omega}$, to the right hand side of the scaling function Eq. (12) [48, 51, 63]. But the computational complexity prevents us from obtaining statistically accurate results on larger lattice size, $L \geq 15$. Therefore, based on our current numerical results, we conclude that the semi-metal to CDW transition in the attractive $SU(3)$ Hubbard model belongs to the $N_s = 4$ chiral Ising universality class, which is in the same universality class with the spinless model described by Eq. (7).

D. Trion formations

In this section, we further investigate the CDW phase from the trion formations. To study the local bound state in the CDW phase, we first define the probability distribution [64, 65],

$$T(i, j) = \langle n_{i1} n_{j2} n_{j3} \rangle, \quad (13)$$

which measures the double occupancy of fermions with flavors $\alpha = 2, 3$ on site j provided that the fermion with the flavor $\alpha = 1$ is on the *reference* site i . As shown in Fig. 7, we choose a reference site \circ to show the value of $T(\circ, j)$ on the $L = 9$ honeycomb lattice. In the semi-metal phase such as $U = -0.5$, the peak of $T(\circ, j)$ is localized on the reference site and the nearest-neighbors of the reference site have the lowest value of $T(\circ, j)$ with imbalance between two sublattices. Tuning the attractive interaction to $U = -1.5$ near the critical point, the imbalance between two sublattices is further enhanced. In the CDW phase at $U = -3$, the long-range correlated charge density imbalance is formed, but the probability on the other sublattice bears a non-zero value, which negates the ordering of pure *on-site* trionic CDW in the early stage of CDW phase.

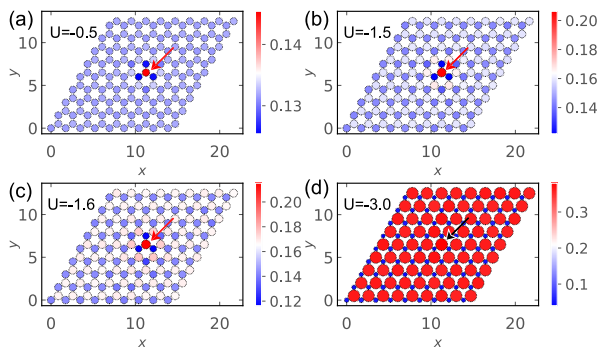


FIG. 7. Probability distribution $T(\circ, j) = \langle n_{\circ 1} n_{j 2} n_{j 3} \rangle$ of the double occupancy with flavors $\alpha = 2, 3$ on the $L = 9$ honeycomb lattice. The circle marker represents the lattice site and its size is proportional to the double occupancy probability. The colorbar is also related to the double occupancy probability on each site. The reference site \circ is pointed by an arrow as guide to eyes.

In order to illustrate the on-site trion formation process with respect to the attractive interaction, we next define the local probability function by averaging the local correlations that measures the trion number (occupancy probability) over the entire lattice [66],

$$P(3) = \frac{1}{2L^2} \sum_i T(i, i). \quad (14)$$

Due to the particle-hole symmetry at half filling, the probability functions $P(n)$ for other occupations have the equivalence relations: $P(0) = P(3)$, $P(1) = P(2)$ and $P(2) + P(3) = \frac{1}{2}$ where n in $P(n)$ is the occupation number. At the non-interacting limit, the on-site density-density correlation between distinct flavors can be decoupled directly, so the probability distribution obeys the binomial distribution: $\lim_{U \rightarrow 0} P(3) = \frac{1}{8}$ and $\lim_{U \rightarrow 0} P(2) = \frac{3}{8}$. In the strong coupling limit $|U| \rightarrow \infty$, three fermions tend to bound together to form a trion composite as shown in Fig. 1(a), so we have $\lim_{|U| \rightarrow \infty} P(3) = \frac{1}{2}$ and $\lim_{|U| \rightarrow \infty} P(2) = 0$ where all sites are either fully occupied (trion) or empty.

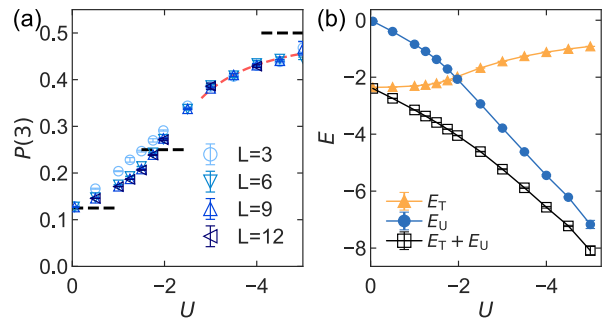


FIG. 8. (a) Probability distribution of the on-site trion occupancy as a function of U for finite lattice sizes $L = 3, 6, 9$ and 12 . Due to the particle-hole symmetry at half filling, $P(0) = P(3)$ (blue color) and $P(2) = \frac{1}{2} - P(3)$ (not shown). The black color dashed horizontal line on the left(right) corner is the limit value $P(3) = \frac{1}{8}(\frac{1}{2})$ at the weak(strong) coupling limit. The horizontal line in the middle denotes the value $P(3) = P(2) = \frac{1}{4}$. The red color dashed curve is a least-square fit to the data points with $0.5 - C_0 \frac{1}{|U|^2}$ in $|U| \geq 3$. (b) The hopping energy E_T (orange solid line) and the on-site interaction $E_U \equiv U \sum_{\alpha < \beta} \langle n_{i\alpha} n_{i\beta} \rangle$ (blue solid line) as the function of $|U|$ for lattice size $L = 9$, averaged on $2L^2$ sites.

Fig. 8(a) shows that values of $P(3)$ on $L = 6, 9$ and 12 honeycomb lattices are hardly distinguishable, so we assume that lattice sizes $L \geq 9$ are sufficient to convey some thermodynamic property of $P(n)$. With increasing $|U|$, $P(3)$ increases monotonically starting from the weak coupling limit $\frac{1}{8}$ to the strong coupling limit $\frac{1}{2}$. On the other hand, $P(2)$ would decrease monotonically and a crossing, $P(3) = P(2) = \frac{1}{4}$, is observed at $U \approx -1.84$. Meanwhile, according to Eq. (7), the trion on each site has the effective hopping amplitude proportional to $\frac{1}{|U|^2}$ indicating that the kinetic energy gain would approach to zero. As shown in Fig. 8(b), the hopping energy indeed shows the tendency towards zero, which is a property of the localized Mott insulator.

We find $P(3)$ follows the equation $P(3) = 0.5 - C_0 \frac{1}{|U|^2}$ in the range of $|U| \geq 3$. The fitting parameter is $C_0 = 1.10(3)$ and the red color dashed curve in Fig. 8(a) shows a good agreement. One can easily deduce a similar proportional relation between the occupation number and the coupling strength, $P(3) = 0.5 - \frac{3}{8} \frac{1}{|U|^2}$, for a two-sites model at strong coupling, but $C_0 > \frac{3}{8}$. The two-sites model underestimates the probability of double occupancy by ignoring the CDW order on a honeycomb lattice. At strong coupling, we do not expect the nearest-neighbor hopping process of single fermion to induce the double occupancy as in the semi-metal phase. Preferably, we assume the finite value of $P(2)$ comes from the *off-site* trion formation [64]. We use the notation $|P_3\rangle$ to denote the on-site trion state and $|P_2\rangle$ as the off-site trion case. The Hamiltonian of Eq. (1) has the matrix form in the

subspace spanned by the basis $\{|P_2\rangle, |P_3\rangle\}$,

$$H = \begin{bmatrix} (-U/2 - 2t)L^2 & -3tL^2 \\ -tL^2 & (3U/2)L^2 \end{bmatrix}. \quad (15)$$

The eigenstate in the subspace with the lowest eigenvalue is $|\lambda\rangle = C_2|P_2\rangle + C_3|P_3\rangle$. Therefore, the probability to form the trion on one site is $P(3) = \frac{C_3^2}{2}$, and the probability to break the on-site trion is $P(2) = \frac{C_2^2}{2}$. We show the series expansion of $P(3)$ in the strong coupling limit,

$$P(3) = \frac{1}{2} - \frac{9t^2}{8U^2} + O\left[\frac{t}{U}\right]^3, \quad (16)$$

where $\frac{9}{8} = 1.125$ quantitatively agrees with the fitting parameter $C_0 = 1.10(3)$. Here, the underlying assumption and the numerical confirmation in addition to the spatial arrangement as shown in Fig. 7 support that the on-site trionic CDW state and the off-site trionic CDW state coexist in the CDW regime.

IV. CONCLUSIONS AND DISCUSSIONS

In this paper, we studied the half-filled attractive SU(3) Hubbard model on a honeycomb lattice at zero temperature using projector quantum Monte Carlo method for the first time. We focused on the intermediate interaction regime where the mean-field theory and perturbative theory may fail. The low-energy physics of this system is described by Dirac fermions and it shows a quantum phase transition from a semi-metallic state to a CDW state. On the other hand, the (color) superfluid phase is absent in this system, which means there is no breaking SU(3) symmetry.

We investigated the critical behavior of the semi-metal to CDW transition and showed the similarity to its effective model, a spinless fermion model with nearest-neighbor hopping and nearest-neighbor repulsive interaction. Though the enlarged computational complexity yet restricts the simulation to concern bigger lattice sizes in this paper, the adequate numerical proofs on lattices containing up to 288 sites support the quantum phase transition belongs to the $N_s = 4$ chiral Ising universality class that the same one for the effective spinless fermion model by the critical exponents $\nu = 0.82(3)$, $\eta = 0.58(4)$, and the critical point $U_c = -1.52(2)$.

We also demonstrated the trion formation with respect to the attractive interaction. We displayed the trion occupancy as well as the charge density imbalance on a honeycomb lattice at half filling. The on-site trion occupancy probability shows a nice proportional relation to $\frac{1}{U^2}$. Together with the spatial imbalance of the charge density, we showed the CDW phase should be understood as the coexistence of on-site trionic and off-site trionic CDW state.

Here, we should remark that the lattice size in our simulation is relatively small and is difficult to be very

decisive on the universality class of the phase transition. We notice that the ‘‘half filling’’ condition can be crucial for many properties of this system such as the absence of SF ordering, the similarity to the effective model and the existence of the off-site trionic CDW state. Therefore, the model away from half filling may show a richer phase diagram.

ACKNOWLEDGMENTS

This work is financially supported by the National Natural Science Foundation of China under Grants No. 11874292, No. 11729402, No. 11574238, and No. 11874312. X. W. also acknowledges the support from Research Grants Council of the Hong Kong Special Administrative Region, China (No. CityU 11303617), and the Guangdong Innovative and Entrepreneurial Research Team Program (No. 2016ZT06D348). L. W. is supported by the Ministry of Science and Technology of China under the Grants No. 2016YFA0300603 and No. 2016YFA0302400. This work made use of the facilities of Tianhe-2 at the China’s National Supercomputing Centre in Guangzhou. We also acknowledge the support of the Supercomputing Center of Wuhan University.

Appendix A: The auxiliary fields couple to on-site flavor flp

For simplicity, we demonstrate the derivation on the finite temperature formalism. We first apply the Suzuki-Trotter decomposition to separate the kinetic part and on-site interaction, and obtain the partition function Z ,

$$Z = \text{tr} e^{-\beta H} = \text{tr} \left[\prod_k^M e^{-\Delta\tau H_0} e^{-\Delta\tau H_I} \right] + O(\Delta\tau^2), \quad (A1)$$

where $\Delta\tau = \frac{\beta}{M}$ is the discrete imaginary-time interval. For the Hubbard interaction part,

$$\begin{aligned} & e^{-\Delta\tau U \sum_{\alpha<\beta} (n_{i\alpha} - \frac{1}{2})(n_{i\beta} - \frac{1}{2})} \\ &= \prod_{\alpha<\beta} e^{-\frac{\Delta\tau U}{2} (c_{i\alpha}^\dagger c_{i\beta} - \text{h.c.})^2 - \frac{\Delta\tau U}{4}}, \end{aligned} \quad (A2)$$

we rewrite the coupling between flavor α and β as

$$\begin{pmatrix} c_\alpha^\dagger & c_\beta^\dagger \end{pmatrix} \begin{pmatrix} 0 & 1 \\ -1 & 0 \end{pmatrix} \begin{pmatrix} c_\alpha \\ c_\beta \end{pmatrix}, \quad (A3)$$

which is diagonalized in the new basis with complex fermion operators [52],

$$\tilde{c}_{\alpha\beta} = \frac{1}{\sqrt{2}}(c_\alpha - ic_\beta), \quad \tilde{c}_{\beta\alpha} = \frac{1}{\sqrt{2}}(c_\alpha + ic_\beta). \quad (A4)$$

We verify that the operators $\tilde{c}_{\alpha\beta}, \tilde{c}_{\beta\alpha}$ obey fermionic commutations, $\{\tilde{c}_{\alpha\beta}^\dagger, \tilde{c}_{\alpha\beta}\} = 1$, $\{\tilde{c}_{\alpha\beta}^\dagger, \tilde{c}_{\beta\alpha}\} = 0$. With

the diagonal form of Eq. (A3), the coupling term $(c_\alpha^\dagger c_\beta - c_\beta^\dagger c_\alpha)^2$ between flavor α and β in Eq. (A2) becomes $-(\tilde{c}_{\alpha\beta}^\dagger \tilde{c}_{\alpha\beta} - \tilde{c}_{\beta\alpha}^\dagger \tilde{c}_{\beta\alpha})^2$. We construct the discrete Hubbard-Stratonovich (HS) transformation on the subspace of the complex basis,

$$e^{\frac{\Delta\tau U}{2}(\tilde{c}_{\alpha\beta}^\dagger \tilde{c}_{\alpha\beta} - \tilde{c}_{\beta\alpha}^\dagger \tilde{c}_{\beta\alpha})^2} = \frac{1}{2} \sum_{s_{\alpha\beta}=\pm 1} e^{is_{\alpha\beta}\lambda(\tilde{c}_{\alpha\beta}^\dagger \tilde{c}_{\alpha\beta} - \tilde{c}_{\beta\alpha}^\dagger \tilde{c}_{\beta\alpha})}, \quad (\text{A5})$$

where $\lambda = \arccos e^{\frac{\Delta\tau U}{2}}$, $U < 0$. Then, in the original basis in Eq. (A2), the following HS transformation will hold,

$$e^{-\Delta\tau U(n_\alpha - \frac{1}{2})(n_\beta - \frac{1}{2})} = \frac{1}{2} e^{-\frac{\Delta\tau U}{4}} \sum_{s_{\alpha\beta}=\pm 1} e^{s_{\alpha\beta}\lambda(c_\alpha^\dagger c_\beta - c_\beta^\dagger c_\alpha)}. \quad (\text{A6})$$

In order to have an effective Hamiltonian in the explicit form of anti-symmetric matrix that on the exponential, we decouple the three Hubbard interaction terms from the density channel to the on-site flavor-flip channel by introducing three auxiliary fields s_{12}, s_{13}, s_{23} ,

$$e^{-\Delta\tau U \sum_{\alpha<\beta} (n_\alpha - \frac{1}{2})(n_\beta - \frac{1}{2})} = \frac{1}{8} e^{-\frac{3\Delta\tau U}{4}} \sum_{s_{12}, s_{13}, s_{23}=\pm 1} e^{\sum_{\alpha<\beta} s_{\alpha\beta}\lambda(c_\alpha^\dagger c_\beta - c_\beta^\dagger c_\alpha)}, \quad (\text{A7})$$

which induces the systematic error of order $\mathcal{O}(\Delta\tau^2)$. As shown in Fig. 9, we expand two side of Eq. (A7) on the *on-site* Fock space and apply the error analysis about the diagonal terms of the matrices. Consequently, the QMC procedure in this work should be accurate in the intermediate interaction regime but debatable at the strong coupling.

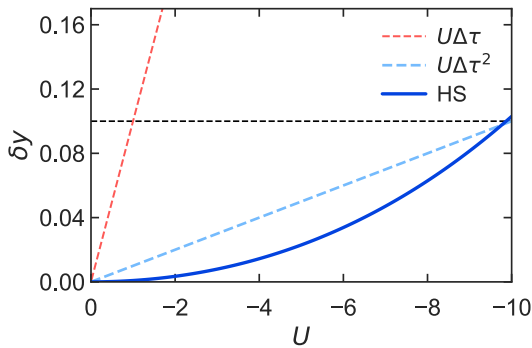


FIG. 9. Correctness test of the HS decomposition. The blue solid curve shows the results with Suzuki-Trotter discretization $\Delta\tau = 0.1$. For comparison, two standard forms of the discretization error: $\Delta\tau$ and $\Delta\tau^2$, are drawn in red dashed line and light blue dashed line, respectively.

Next, we show that QMC using the decomposition of Eq. (A7) can avoid the sign problem. On the bipartite lattice, we arrange the flavor-orbital operators in two

sublattices in such order: $A_\alpha, A_\beta, A_\gamma; B_\alpha, B_\beta, B_\gamma$. Correspondingly, the effective single-particle Hamiltonian has the kind of structure, $H_k = \begin{pmatrix} D_A & K \\ K & D_B \end{pmatrix}$, where K represents the hopping between two sublattices and $D_{A(B)}$ is a block diagonal matrix. Each block in $D_{A(B)}$ is an anti-symmetric matrix,

$$\Lambda = \begin{pmatrix} 0 & s_{12}\lambda & s_{12}\lambda \\ -s_{12}\lambda & 0 & s_{23}\lambda \\ -s_{13}\lambda & -s_{23}\lambda & 0 \end{pmatrix}, \quad (\text{A8})$$

and $\Lambda^T = -\Lambda$. It is direct to prove the effective single-particle Hamiltonian satisfy the relation of $\eta H_k \eta = -H_k^T$ where the matrix $\eta = \text{diag}(\underbrace{1, \dots, 1}_n, \underbrace{-1, \dots, -1}_n)$, which

guarantees the determinantal QMC simulations to be sign-problem-free [33]. When the system is away from the half-filling condition, the matrix $D_{A(B)}$ is not real anti-symmetric, which will cause the sign problem. We can use the Rodrigues formula on each Λ to generate the matrix exponential of $D_{A(B)}$ by calculating each diagonal block $e^\Lambda = I_3 + \frac{\sin\theta}{\theta}\Lambda + \frac{(1-\cos\theta)}{\theta^2}\Lambda^2$ where $\theta = \sqrt{(s_{12}^2 + s_{13}^2 + s_{23}^2)\lambda^2} = \sqrt{3}\lambda^2$.

In general, this type of on-site flavor flip decomposition can be generalised from SU(3) to SU(2N+1) half-filled Hubbard model. The shortcoming of this decomposition is the increase of matrix size which has the $\beta(2L^2N)^3$ scaling. N is the number of flavor and $2L^2$ is the number of sites on a honeycomb lattice. The HS decomposition of Eq. (A7) can also be applied to the PQMC method, and the only modification is about studying the expectations on the zero-temperature ground state $|\Psi_G\rangle$ instead of the partition function Eq. (A1), for example the CDW structure factor $\langle\Psi_G|S_{\text{CDW}}|\Psi_G\rangle$. We can choose a trial wave function $|\Psi_T\rangle$ as the ground state of the single-particle Hamiltonian, Eq. (1) with $U = 0$, with anti-periodic boundary condition to avoid sign problem [33]. Given that the inner product $\langle\Psi_G|\Psi_T\rangle \neq 0$, the ground state $|\Psi_G\rangle$ will be reached by applying the projection operator $e^{-\frac{\beta H}{2}}$ on $|\Psi_T\rangle$ with the projection time $\beta \rightarrow \infty$ [42, 67].

Here we show the comparison to the exact diagonalization (ED) solution of the attractive SU(3) Hubbard on a 2×2 square lattice with periodic boundary condition. The choices of projection time $\beta = 10, 20$ are drawn for comparison. As shown in Fig. 10, for most of the cases, PQMC gives the exact result of the ED calculation within the margin of numerical error. However, at $U = -0.05$, we seemingly obtain a contradictory result. The reason is that near the Fermi surface nesting, our choice of trial wave function may become inappropriate and triggers the slow convergence towards the ground state.

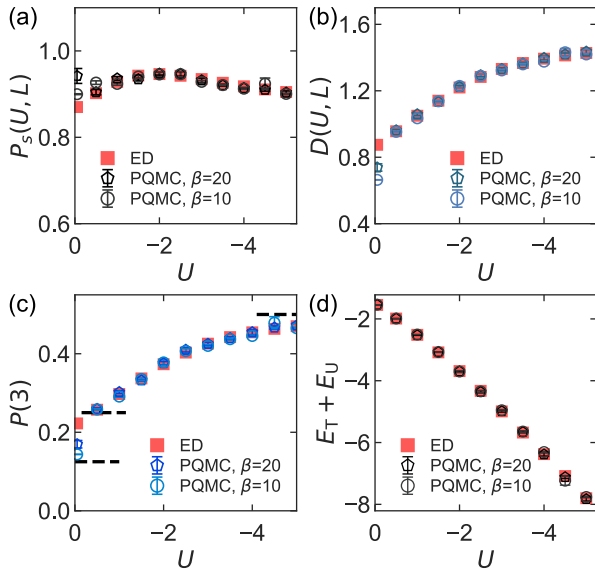


FIG. 10. Correctness test on a 2×2 square lattice. The exact diagonalization results is shown as the red color square marker. PQMC results with Suzuki-Trotter discretization $\Delta\tau = 0.1$ and two kinds of projection time $\beta = 10, 20$ are drawn. (a) The SF order parameter. (b) The CDW order parameter. (c) The trion occupancy probability. (d) The total energy consists of the hopping term E_T and the on-site interaction E_U as defined in the main text.

Appendix B: Unequal-time correlation functions

The CDW ordering will open a single-particle gap in the dispersion spectrum at the Dirac point [68]. At mean-field consideration, the gap lifted by the charge density imbalance is $2U\Delta$ at the Dirac point. Here, we study the unequal-time correlation functions,

$$G_{\mathbf{k}}(\tau) = \frac{1}{2L^2} \sum_{ij} G_{ij}(\tau) e^{i\mathbf{k}\cdot\mathbf{r}_{ij}}, \quad (\text{B1})$$

where \mathbf{r}_{ij} is the spatial vector between site i and site j , $G_{ij}(\tau) = \langle \sum_{\alpha\beta} e^{\tau\hat{H}} c_{i\alpha} e^{-\tau\hat{H}} c_{j\beta}^\dagger \rangle$ is the unequal-time Green function. Based on Eq. (B1), we give the formal definition of a spectral function $A(\omega)$ by applying the analytic continuation to the frequency representation,

$$G_{\mathbf{k}}(\tau) = \int_{-\infty}^{+\infty} d\omega \mathcal{K}(\tau, \omega) A(\omega), \quad (\text{B2})$$

with $\mathcal{K}(\tau, \omega) = \theta(\omega) e^{-\tau\omega}$ at zero temperature, $\theta(\omega)$ being the Heaviside step function [69, 70]. The peaks of $A(\omega)$ can be a function of ω and \mathbf{k} , which represents the dispersion relation $\omega(\mathbf{k})$ of quasi-particle excitations [71].

Here we show the dispersion relation along the path on the reciprocal lattice: $\Gamma \rightarrow K \rightarrow M \rightarrow K' \rightarrow \Gamma \rightarrow M$, where K, K' are the Dirac points, M is the site in middle of K and K' . As shown in Fig. 11, the low-energy spectrum is modified as the attractive interaction increases. Fig. 11(b) shows that there is no gap opening

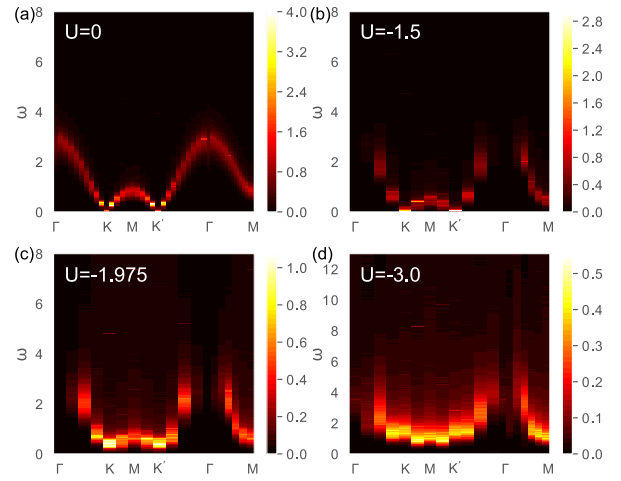


FIG. 11. The spectral function $A(\omega)$, using analytic continuation on $G_{\mathbf{k}}(\tau)$ obtained from: (a) The non-interacting limit, $U = 0$, on the $L = 30$ honeycomb lattice. (b)-(d) the PQMC simulation on a honeycomb lattice of size $L = 12$. The calculation is based on the GPU code published in [70].

at Dirac points at $U = -1.5$, which is consistent with the critical value $U = -1.52(2)$ in the main text. After entering the CDW phase, the single-particle gap opens at K, K' points. In the QMC simulation, the numerical data can drop to approximately equal to zero very quickly because of a large single-particle gap, which causes the difficulty in calculating the dispersion relation at the Γ point. A smaller Suzuki-Trotter discretization $\Delta\tau$ may resolve this problem.

Appendix C: Estimation of the single particle gap

The Hamiltonian can be split into two parts, $\hat{H} = \hat{H}_U + \hat{H}_K$ where $\hat{H}_U = U \sum_{i,\alpha < \beta} (\hat{n}_{i\alpha} - 1/2)(\hat{n}_{i\beta} - 1/2)$ and $\hat{H}_K = -t \sum_{\langle ij \rangle, \alpha} (\hat{c}_{i\alpha}^\dagger \hat{c}_{j\alpha} + h.c.)$. At the strong coupling limit ($t/|U| \rightarrow 0$), N fermions form a local bound color singlet in one sublattice namely Λ_t , leaving the other sublattice empty. The density wave order breaks the ground state degeneracy of the atomic limit ($t = 0$) in the half-filled system suggested by the second-order perturbation [28]. Normally, we use the single-particle gap to denote the Mott-insulating phase which is equivalent to the particle fluctuations of adding or removing a particle which needs an energy [72, 73]. First, we consider the energy scale of adding an extra hole (particle) onto the Mott-insulating state in the atomic limit: $\Delta_E = E_{N_{\text{tot}}-1} - E_{N_{\text{tot}}} = -\frac{U}{2}(N-1)$ with N_{tot} the total number of fermions. After tuning on the hopping term, the ground state of the nearly half-filled system holds a competition between density wave and superfluid order [22, 30, 74]. Instead of providing a compact solution to the ground state of the nearly half-filled case, we focus on providing an approximation for the value of the crit-

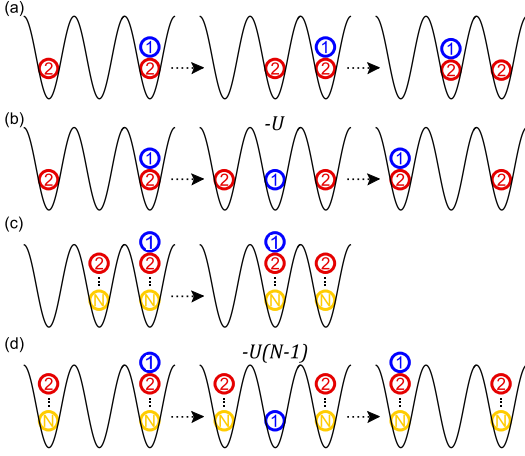


FIG. 12. Adding an extra hole to the half-filled SU(2) system, (a) shows the hopping processes inside the subspace \mathcal{D} i.e. the degenerate ground states at atomic limit. (b) shows one of the second-order hopping processes. The middle configuration lifts the energy by $-U$. For the SU(N) model with $N > 2$, (c) shows the hopping process inside the degenerate subspace \mathcal{D} . (d) shows a second-order hopping process where the middle configuration lifts the energy by $-U(N-1)$.

ical U_c . This can be achieved through forming a s -band tight-binding model about the extra hole (particle) hopping to the next-nearest-neighbor (NNN) sites which can be treated in the standard degenerate perturbation calculation, .

Let us calculate the effective Hamiltonian for the nearly half-filled system. Following the textbook steps [75], we define the ground state $|n^{(0)}\rangle$ by $\hat{H}_U|n^{(0)}\rangle = E_D^{(0)}|n^{(0)}\rangle$ with $E_D^{(0)} = E_{N_{\text{tot}}-1}$. Take \hat{P}_0 as the projection operator onto the subspace \mathcal{D} of the ground states. $\hat{P}_1 = 1 - \hat{P}_0$ thus gives the projection outside the subspace \mathcal{D} . The degenerate Rayleigh-Schrödinger perturbation theory yields the effective Hamiltonian, $\hat{H}_{\text{eff}}|n^{(0)}\rangle = E_n|n^{(0)}\rangle$, up to the second order,

$$\hat{H}_{\text{eff}} = \hat{P}_0 \left(E_D^{(0)} + \hat{H}_K + \hat{H}_K \hat{P}_1 \frac{1}{E_D^{(0)} - \hat{H}_U} \hat{P}_1 \hat{H}_K \right) \hat{P}_0. \quad (\text{C1})$$

Here, the hopping operator $\hat{H}_K \hat{P}_0$ brings one fermion in the local bound singlet to the nearest-neighbor site causing an energy difference, as shown in Fig. 12. Taking the Pauli exclusion principle into consideration, we rewrite the Hamiltonian as

$$\hat{H}_{\text{eff}} = E_D^{(0)} + C^{(1)} + C^{(2)}(z) + \frac{t^2}{U(N-1)} \hat{P}_0 \sum_{\langle\langle ij \rangle\rangle \in \Lambda_{t,\alpha}} (\hat{c}_{i\alpha}^\dagger \hat{c}_{j\alpha} + \text{h.c.}) \hat{P}_0, \quad (\text{C2})$$

$$= E_{N_{\text{tot}}-1} + C^{(1)} + C^{(2)}(z) + \frac{t^2}{U(N-1)} \sum_{\langle\langle ij \rangle\rangle \in \Lambda_t} (\hat{c}_i^\dagger \hat{c}_j + \text{h.c.}), \quad (\text{C3})$$

$$= E_{N_{\text{tot}}-1} + C^{(1)} + C^{(2)}(z) + \sum_{\mathbf{k}} \epsilon_t(\mathbf{k}) \hat{c}_{\mathbf{k}}^\dagger \hat{c}_{\mathbf{k}}, \quad (\text{C4})$$

where $C^{(1)} = \hat{P}_0 \hat{H}_K \hat{P}_0$ is the first-order perturbation and $C^{(2)}$ is the remaining second-order perturbation that one fermion hops to the nearest-neighbor sites but returns back. The $C^{(2)}$ term is related to the lattice structure, which is a function of the coordination number z . The effective tight-binding model is originated from the second-order process shown in Fig. 12(d), $\langle\langle ij \rangle\rangle$ represents the NNN sites, $\epsilon_t(\mathbf{k})$ is the dispersion relation depending on the lattice structure and the NNN hopping is restricted in one flavor channel that is determined by the extra hole (particle). For the ground state, it's natural to assume the extra hole (particle) takes the lowest energy level: $\epsilon_t(\mathbf{k}_0) = -yt'$ where $t' = -\frac{t^2}{U(N-1)}$ and $y > 0$ is a constant relying on the lattice structure.

Following similar arguments, the second-order perturbation on the half-filled system yields $\hat{H}_{\text{eff}} = E_{N_{\text{tot}}} + \tilde{C}^{(2)}(z)$ where the NNN hopping is not permitted in the second-order perturbation. Therefore the energy scale af-

ter tuning on the hopping term reads,

$$\Delta_E = -\frac{U}{2}(N-1) + \frac{yt^2}{U(N-1)} + C^{(1)} + \Delta C^{(2)}(z), \quad (\text{C5})$$

where $\Delta C^{(2)}(z) \sim \frac{t^2}{U}$ is the difference in the second-order correction terms. The $\Delta_E = 0$ condition in the above function deduces the critical value of the Mott transition. If we discard both $C^{(1)}$ and $\Delta C^{(2)}$, we obtain the approximation for the critical point,

$$U_c/t = -\frac{\sqrt{2y}}{N-1}. \quad (\text{C6})$$

Note that what we discarded can further reduce the energy scale, so the real critical value $|U_c|/t$ should be smaller compared to Eq. (C6). For the SU(3) Hubbard model on the honeycomb lattice, the number of fermion components is $N = 3$ and $\epsilon_t(\mathbf{k})$ is on the triangular lat-

tice,

$$\epsilon_t(\mathbf{k}) = -2t' \sum_{i=1}^3 \cos(\mathbf{k} \cdot \boldsymbol{\delta}_i), \quad (\text{C7})$$

where the vectors $\boldsymbol{\delta}_1 = (\sqrt{3}a, 0)$, $\boldsymbol{\delta}_2 = (-\frac{\sqrt{3}}{2}a, \frac{3}{2}a)$ and

$\boldsymbol{\delta}_3 = (\frac{\sqrt{3}}{2}a, -\frac{3}{2}a)$ with a the lattice constant of the honeycomb lattice. We then deduce the lowest energy level $\epsilon_t(\mathbf{k}_0) = -6t'$ and $y = 6$. Inserting the above results into Eq. (C6), we obtain $U_c/t = -\frac{2\sqrt{3}}{2} \approx -1.73$.

-
- [1] I. Affleck and J. B. Marston, *Phys. Rev. B* **37**, 3774 (1988).
- [2] D. P. Arovas and A. Auerbach, *Phys. Rev. B* **38**, 316 (1988).
- [3] N. Read and S. Sachdev, *Phys. Rev. B* **42**, 4568 (1990).
- [4] N. Read and S. Sachdev, *Phys. Rev. Lett.* **66**, 1773 (1991).
- [5] S. Sachdev and N. Read, *International Journal of Modern Physics B* **5**, 219 (1991).
- [6] S. Taie, Y. Takasu, S. Sugawa, R. Yamazaki, T. Tsujimoto, R. Murakami, and Y. Takahashi, *Phys. Rev. Lett.* **105**, 190401 (2010).
- [7] B. J. DeSalvo, M. Yan, P. G. Mickelson, Y. N. Martinez de Escobar, and T. C. Killian, *Phys. Rev. Lett.* **105**, 030402 (2010).
- [8] S. Taie, R. Yamazaki, S. Sugawa, and Y. Takahashi, *Nature Physics* **8**, 825 (2012).
- [9] F. Scazza, C. Hofrichter, M. Höfer, P. De Groot, I. Bloch, and S. Fölling, *Nature Physics* **10**, 779 (2014).
- [10] X. Zhang, M. Bishof, S. L. Bromley, C. V. Kraus, M. S. Safronova, P. Zoller, A. M. Rey, and J. Ye, *science* **345**, 1467 (2014).
- [11] G. Pagano, M. Mancini, G. Cappellini, P. Lombardi, F. Schäfer, H. Hu, X.-J. Liu, J. Catani, C. Sias, M. Inguscio, *et al.*, *Nature Physics* **10**, 198 (2014).
- [12] M. A. Cazalilla and A. M. Rey, *Reports on Progress in Physics* **77**, 124401 (2014).
- [13] C. Hofrichter, L. Riegger, F. Scazza, M. Höfer, D. R. Fernandes, I. Bloch, and S. Fölling, *Phys. Rev. X* **6**, 021030 (2016).
- [14] C. Wu, J.-p. Hu, and S.-c. Zhang, *Phys. Rev. Lett.* **91**, 186402 (2003).
- [15] C. Honerkamp and W. Hofstetter, *Phys. Rev. B* **70**, 094521 (2004).
- [16] C. Wu, *Phys. Rev. Lett.* **95**, 266404 (2005).
- [17] A. V. Gorshkov, M. Hermele, V. Gurarie, C. Xu, P. S. Julienne, J. Ye, P. Zoller, E. Demler, M. D. Lukin, and A. Rey, *Nature physics* **6**, 289 (2010).
- [18] E. R. I. Abraham, W. I. McAlexander, J. M. Gerton, R. G. Hulet, R. Côté, and A. Dalgarno, *Phys. Rev. A* **55**, R3299 (1997).
- [19] M. Bartenstein, A. Altmeyer, S. Riedl, R. Geursen, S. Jochim, C. Chin, J. H. Denschlag, R. Grimm, A. Simoni, E. Tiesinga, C. J. Williams, and P. S. Julienne, *Phys. Rev. Lett.* **94**, 103201 (2005).
- [20] T. Fukuhara, Y. Takasu, M. Kumakura, and Y. Takahashi, *Phys. Rev. Lett.* **98**, 030401 (2007).
- [21] J. H. Huckans, J. R. Williams, E. L. Hazlett, R. W. Stites, and K. M. O'Hara, *Phys. Rev. Lett.* **102**, 165302 (2009).
- [22] A. Rapp, G. Zaránd, C. Honerkamp, and W. Hofstetter, *Phys. Rev. Lett.* **98**, 160405 (2007).
- [23] A. Rapp, W. Hofstetter, and G. Zaránd, *Phys. Rev. B* **77**, 144520 (2008).
- [24] K. Inaba and S.-i. Suga, *Phys. Rev. A* **80**, 041602 (2009).
- [25] Z. Fodor and S. D. Katz, *Journal of High Energy Physics* **2002**, 014 (2002).
- [26] Y. Aoki, G. Endrődi, Z. Fodor, S. Katz, and K. Szabo, *Nature* **443**, 675 (2006).
- [27] F. Wilczek, *Nature Physics* **3**, 375 (2007).
- [28] I. Titvinidze, A. Privitera, S.-Y. Chang, S. Diehl, M. A. Baranov, A. Daley, and W. Hofstetter, *New Journal of Physics* **13**, 035013 (2011).
- [29] H. Yanatori and A. Koga, *Journal of the Physical Society of Japan* **85**, 014002 (2016).
- [30] G. Klingschat and C. Honerkamp, *Phys. Rev. B* **82**, 094521 (2010).
- [31] A. Moreo and D. J. Scalapino, *Phys. Rev. Lett.* **66**, 946 (1991).
- [32] K. L. Lee, K. Bouadim, G. G. Batrouni, F. Hébert, R. T. Scalettar, C. Miniatura, and B. Grémaud, *Phys. Rev. B* **80**, 245118 (2009).
- [33] L. Wang, Y.-H. Liu, M. Iazzi, M. Troyer, and G. Harcos, *Phys. Rev. Lett.* **115**, 250601 (2015).
- [34] Z. C. Wei, C. Wu, Y. Li, S. Zhang, and T. Xiang, *Phys. Rev. Lett.* **116**, 250601 (2016).
- [35] Z.-X. Li, Y.-F. Jiang, and H. Yao, *Phys. Rev. Lett.* **117**, 267002 (2016).
- [36] A. Koga and H. Yanatori, *Journal of the Physical Society of Japan* **86**, 034702 (2017).
- [37] E. Jones, T. Oliphant, P. Peterson, *et al.*, "SciPy: Open source scientific tools for Python," (2001-).
- [38] R. P. Brent, *Algorithms for minimization without derivatives* (Courier Corporation, 2013).
- [39] S. Sorella and E. Tosatti, *EPL (Europhysics Letters)* **19**, 699 (1992).
- [40] R. Blankenbecler, D. J. Scalapino, and R. L. Sugar, *Phys. Rev. D* **24**, 2278 (1981).
- [41] J. E. Hirsch, *Phys. Rev. B* **31**, 4403 (1985).
- [42] F. Assaad and H. Evertz, "World-line and determinantal quantum monte carlo methods for spins, phonons and electrons," in *Computational Many-Particle Physics*, edited by H. Fehske, R. Schneider, and A. Weiße (Springer Berlin Heidelberg, Berlin, Heidelberg, 2008) pp. 277-356.
- [43] E. Zhao and A. Paramekanti, *Phys. Rev. Lett.* **97**, 230404 (2006).
- [44] L. Wang, P. Corboz, and M. Troyer, *New Journal of Physics* **16**, 103008 (2014).
- [45] Z.-X. Li, Y.-F. Jiang, and H. Yao, *New Journal of Physics* **17**, 085003 (2015).
- [46] F. F. Assaad and I. F. Herbut, *Phys. Rev. X* **3**, 031010 (2013).

- [47] Y. Otsuka, K. Seki, S. Sorella, and S. Yunoki, *Phys. Rev. B* **98**, 035126 (2018).
- [48] Y. Otsuka, S. Yunoki, and S. Sorella, *Phys. Rev. X* **6**, 011029 (2016).
- [49] D. J. Gross and A. Neveu, *Phys. Rev. D* **10**, 3235 (1974).
- [50] B. Ihrig, L. N. Mihaila, and M. M. Scherer, *Phys. Rev. B* **98**, 125109 (2018).
- [51] F. Parisen Toldin, M. Hohenadler, F. F. Assaad, and I. F. Herbut, *Phys. Rev. B* **91**, 165108 (2015).
- [52] Z.-X. Li, Y.-F. Jiang, and H. Yao, *Phys. Rev. B* **91**, 241117 (2015).
- [53] K. Binder, *Phys. B Con. Mat.* **43**, 119 (1981).
- [54] S. Pujari, T. C. Lang, G. Murthy, and R. K. Kaul, *Phys. Rev. Lett.* **117**, 086404 (2016).
- [55] O. Melchert, arXiv:0910.5403 (2009).
- [56] A. Sorge, “Pyfssa 0.7.6,” (2015).
- [57] J. Houdayer and A. K. Hartmann, *Phys. Rev. B* **70**, 014418 (2004).
- [58] E. Huffman and S. Chandrasekharan, *Phys. Rev. D* **96**, 114502 (2017).
- [59] L. Rosa, P. Vitale, and C. Wetterich, *Phys. Rev. Lett.* **86**, 958 (2001).
- [60] F. Höfling, C. Nowak, and C. Wetterich, *Phys. Rev. B* **66**, 205111 (2002).
- [61] L. Janssen and I. F. Herbut, *Phys. Rev. B* **89**, 205403 (2014).
- [62] B. Knorr, *Phys. Rev. B* **94**, 245102 (2016).
- [63] K. S. D. Beach, L. Wang, and A. W. Sandvik, [arXiv preprint cond-mat/0505194v1](https://arxiv.org/abs/cond-mat/0505194v1).
- [64] J. Pohlmann, A. Privitera, I. Titvinidze, and W. Hofstetter, *Phys. Rev. A* **87**, 023617 (2013).
- [65] A. Kantian, M. Dalmonte, S. Diehl, W. Hofstetter, P. Zoller, and A. J. Daley, *Phys. Rev. Lett.* **103**, 240401 (2009).
- [66] R. A. Molina, J. Dukelsky, and P. Schmitteckert, *Phys. Rev. A* **80**, 013616 (2009).
- [67] D. Wang, Y. Li, Z. Cai, Z. Zhou, Y. Wang, and C. Wu, *Phys. Rev. Lett.* **112**, 156403 (2014).
- [68] C. Chen, X. Y. Xu, Z. Y. Meng, and M. Hohenadler, *Phys. Rev. Lett.* **122**, 077601 (2019).
- [69] E. Vitali, M. Rossi, L. Reatto, and D. E. Galli, *Phys. Rev. B* **82**, 174510 (2010).
- [70] J. Nordström, J. Schott, I. L. Locht, and I. D. Marco, *SoftwareX* **5**, 178 (2016).
- [71] M. Jarrell and J. E. Gubernatis, *Physics Reports* **269**, 133 (1996).
- [72] Z. Zhou, Z. Cai, C. Wu, and Y. Wang, *Phys. Rev. B* **90**, 235139 (2014).
- [73] Z. Zhou, D. Wang, Z. Y. Meng, Y. Wang, and C. Wu, *Phys. Rev. B* **93**, 245157 (2016).
- [74] C. Honerkamp and W. Hofstetter, *Phys. Rev. Lett.* **92**, 170403 (2004).
- [75] J. J. Sakurai and E. D. Commins, “Modern quantum mechanics, revised edition,” (1995).